Superheater ash deposit ageing – Impact of melt fraction on morphology and chemistry

Balint, Roland; Engblom, Markus; Niemi, Jonne; Hupa, Mikko; Hupa, Leena

Published in:
Fuel

DOI:
10.1016/j.fuel.2023.130386

Published: 01/03/2024

Document Version
Final published version

Document License
CC BY

Fuel 359 (2024) 130386

Contents lists available at ScienceDirect

Fuel

journal homepage: www.elsevier.com/locate/fuel

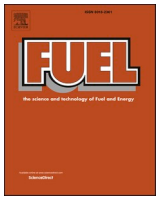

Full Length Article

Superheater ash deposit ageing – Impact of melt fraction on morphology and chemistry

Roland Balint *, Markus Engblom, Jonne Niemi, Mikko Hupa, Leena Hupa

Faculty of Science and Engineering, Åbo Akademi University, Henrikinkatu 2, Turku, FI-20500 Finland

ARTICLE INFO

Keywords:
Ash deposits
Temperature gradient
Melting behavior
Aging mechanisms

ABSTRACT

The initial melting behaviour of synthetic ash deposits, with a focus on how the amount of melt formed, affects the final deposit morphology, was studied. Binary and ternary reciprocal deposits were exposed to a temperature gradient with varying exposure time, steel temperature, and furnace temperature. Two different archetype deposit morphologies emerged. The final deposit morphology was identified to depend on the amount of melt formed during the experiment. A skeletal deposit morphology developed in systems with less than 30 wt-% melt. Short-term experiments proved that the formation of the skeletal structure is accelerated by the presence of melt, accumulating at contact points of distinct particles. If melt fractions exceeded 30 wt-%, a molten morphology developed, as the amount of melt present was sufficient to fill the pores within the deposit. For molten deposits of ternary reciprocal systems, enrichment of K in the formed melt and concurrent movement toward the steel was observed. The results confirmed a deposit ageing mechanism that has been proposed earlier, based on full-scale superheater deposit samples. The experiments showed that deposit melting and ageing behaviour are strongly connected, as the two identified morphologies differed in their ageing behaviour. The presented results improve the understanding of the initial melting behaviour of deposits and illustrate the connection between deposit morphology and deposit ageing. The results can be utilised as input data for deposition models and help in predicting the final deposit morphology and its associated ageing behaviour, aiding boiler operators and manufacturers dealing with deposit-related issues.

1. Introduction

Worldwide, the governing process used in the pulp and paper industry is kraft pulping. The black liquor recovery boiler is an essential part of the kraft pulp mill. Through the combustion of black liquor, the spent pulping chemicals are recovered to be reused. At the same time, heat and power, sufficient to cover the demand of the whole mill [1], are produced. An inevitable part of the combustion process is the release of inorganics in different physical states, which are subsequently entrained in the flue gas and form deposits on heat transfer surfaces via several pathways [2]. Such deposits reduce the electrical efficiency of the process [3] and can also cause corrosion of the heat transfer surfaces they form on [2].

The formation of ash deposits has been studied extensively over the last decades [4–7]. Several deposit formation mechanisms have been identified and studies on different aspects of deposit formation can be found in the literature [3,4,6–8]. The main components of kraft recovery boiler deposits are Na, K, Cl, SO_4, and CO_3 [9]. Of these compounds, alkali chlorides are mainly responsible for superheater corrosion. For solid deposits, the dominating corrosion mechanism is active oxidation [10,11]. If the deposit adjacent to the steel surface is (partially) molten, the corrosion rate increases significantly [6,11,12]. Therefore, a good understanding of the melting behaviour of ash deposits is essential to avoid the presence of melt in the direct vicinity of the steel surface.

The first melting temperature (T_0) of an ash deposit depends on its chemical composition. For kraft recovery boiler deposits, T_0 can be as low as 501 °C when only considering its main components [13]. In addition, smaller amounts of various inorganics originating either from the raw wood [14] or introduced into the liquor during various process steps [14] can be found in the deposits, further affecting T_0. In addition, corrosion products originally formed at the steel surface [15] can be found within deposits, which can form low melting eutectics and increase the risk of melt getting in direct contact with the steel. For kraft recovery boiler deposits, the melting behaviour is mainly influenced by

* Corresponding author at: Laboratory of Molecular Sciences and Engineering, Faculty of Science and Engineering (FNT), Åbo Akademi University, Henriksgatan 2, Åbo, FI-20500 Finland.
E-mail address: roland.balint@abo.fi (R. Balint).

https://doi.org/10.1016/j.fuel.2023.130386
Received 28 April 2023; Received in revised form 31 October 2023; Accepted 11 November 2023
Available online 18 November 2023

the deposit K and Cl content. An increase in the deposit's K content causes a decrease in T_0 [16]. An increase in the deposit's Cl content results in an increase in the amount of melt present within the deposit [17].

Several studies have reported local differences in the chemical composition and morphology of superheater deposits from kraft recovery boilers [17,18], and other biomass boilers [19–21]. Such differences in the local chemical composition of a deposit can also affect the local T_0 [18,22]. A commonly found explanation for why deposits form layered structures of varying chemical composition is a change in the deposition behaviour [21,23]. In literature, a generally accepted pathway of deposit formation is the initial formation of a sticky layer on the blank steel surface via condensation of inorganic vapours [23]. The sticky layer then enables further deposition of larger fly-ash particles which differ in their composition from the initially formed sticky layer [23]. Thus, distinct layers of varying compositions and T_0 can be found within a deposit's cross-section.

Recent studies carried out at Åbo Akademi University have shown that temperature gradient-induced processes can also cause changes in the local chemical composition and morphology of deposits [15,24,25]. Due to the temperature difference between the hotter flue gas and the cooler steel surface, deposits are exposed to a temperature gradient. In laboratory experiments utilising synthetic ash deposits, several temperature gradient-induced mechanisms affecting the local deposit chemistry and morphology have been identified [15,24,25]. Such mechanisms are commonly referred to as deposit ageing, as they take place after the deposit has formed. These mechanisms were later also confirmed to take place in actual kraft recovery boiler superheater deposits [26–28]. In addition, new observations were made within the full-scale deposits. Melt enriching in K and Cl was identified to result in a decrease in the local T_0 of deposits toward the steel [26]. The results are believed to have provided a reasonable explanation for the heavy corrosion, that has earlier been reported for the same boiler [18].

Besides differences in the local chemical composition, significant morphological differences have been observed among deposits from different recovery boilers. Deposits of a generally higher Cl content formed a dense morphology that appeared to have been completely molten. In these dense deposits, K and Cl-enriched melt had moved toward the steel locally lowering T_0 [26]. Deposits of lower Cl content formed a different morphology. The deposits were porous and particles formed a sintered skeletal structure. The porous morphology enabled the diffusion of flue-gas compounds into the deposit, altering the local chemical composition of the inner deposit region [27,28]. The observed differences in the final deposit morphology and therewith connected differences in the ageing behaviour were due to differences in the melting behaviour of the deposits. However, the exact parameters determining the final deposit morphology are not known. Based on the observations made in these earlier studies, the melting behaviour of deposits is believed to affect the final deposit morphology strongly.

The objective of this work was to get a better understanding of the initial melting behaviour of kraft recovery boiler deposits. The main goal was to identify the parameter determining whether the final morphology of a mature deposit is molten or skeletal. Therefore, the initial melting behaviour of synthetic ash deposits was studied in a laboratory setup. Various deposit compositions were exposed to a temperature gradient for short periods, to better understand the initial melt formation and further propagation of the melting processes. The melt fraction present during the experiment was determined by measuring the temperature right above the outer deposit surface. The maximum amount of melt formed during an experiment was identified as the decisive parameter for the final deposit morphology. A threshold value at which the morphology changes from skeletal to molten is proposed.

2. Material and methods

A laboratory setup was used to study the initial steps of the melting behaviour of synthetic ash deposits exposed to a temperature gradient. Varying compositions of deposits containing Na, K, Cl and SO_4 were used. The setup consists of an air-cooled probe which is placed inside a tube furnace. The synthetic deposits were placed on two removable steel rings at the probe tip. Due to the temperature difference between the cooled probe surface and the hotter furnace, a temperature gradient builds up over the synthetic deposit. The synthetic deposits were placed in a mould of fire sealant paste to prevent the molten deposit from flowing off the probe during the experiment. The temperature of the probe was measured and controlled by a thermocouple placed inside one of the sampling rings. A PID regulator adjusted the flow of cooling air within the probe, maintaining a constant steel temperature during the experiment. During the experiment, a second thermocouple was placed inside the tube furnace, measuring and logging the temperature right above the outer deposit surface. The setup has been used earlier, to study the effect of a temperature gradient on synthetic deposits. A more detailed description of the experimental setup can be found in these earlier studies [24,25].

The compositions of the synthetic ash deposits and their corresponding calculated first melting temperatures (T_0) are summarised in Table 1.

The first three synthetic deposits in Table 1 contain only one alkali metal each (binary salt system). The 86-Na_2SO_4 and 77-K_2SO_4 compositions, which have also been used in earlier deposit ageing studies [25], form 20 wt-% melt at T_0 and were chosen to identify possible differences between K and Na-containing deposits. The 69-K_2SO_4 mixture forms 30 wt-% melt at the same T_0 as the 77-K_2SO_4 mixture. The three binary salt mixtures are eutectic systems, in which the local T_0 is not affected by local temperature gradient-induced element enrichment. The four other synthetic deposits are more complex. They contain Na and K salts simultaneously (ternary reciprocal salt system), hence more representative of actual black liquor kraft recovery boiler superheater deposits. The ternary reciprocal salt mixtures vary in their K and Cl content. The compositions were chosen to achieve variation in T_0, T_{100}, and the amount of melt formed at T_0. The ternary reciprocal mixtures aim to cover a variety of melting behaviours possibly occurring in actual recovery boiler deposits.

The salt mixtures were prepared by weighing the single compounds which were subsequently mixed, melted, and ground. This procedure provided a homogeneous distribution of all compounds in the mixture. By this, all local differences in the chemical composition of the deposits can be attributed to being temperature gradient-induced and do not originate from an initially inhomogeneous deposit. The ground particles were sieved to a particle size fraction ranging between 53 and 250 μm, which was used in the experiments. In one experiment, particles smaller than 53 μm were used to study the impact of smaller particles on the deposit melting behaviour. After sieving, the salt compositions were analysed using SEM/EDXA to take into account minor deviations of the used salts from the compositions shown in Table 1. The compositions determined using SEM/EDXA were then used to calculate the respective melting behaviour of the salts.

The melting behaviour of the used deposits was calculated using FactSage 8.1 [29] and the FTPulp database, optimized for compositions representing kraft recovery boiler deposits [13]. The used database contains data relevant to salt mixtures comprising NaCl, KCl, Na_2SO_4,

Table 1
Composition and first melting temperature of synthetic ash deposits.

Synthetic ash	Na [wt-%]	K [wt-%]	Cl [wt-%]	SO_4 [wt-%]	T_0 [°C]
86-Na_2SO_4	33	–	4	63	626
77-K_2SO_4	–	46	5	49	690
69-K_2SO_4	–	46	8	46	690
1 K 1Cl	32	1	1	66	615
10 K 1Cl	25	10	1	64	556
10 K 10Cl	26	10	10	54	557
1 K 10Cl	33	1	10	56	613

K_2SO_4, Na_2CO_3, K_2CO_3, Na_2S, and K_2S. In the calculations the following phases were considered: FTpulp-MELTA (liquid phase), FTpulp-Hexa (hexagonal alkali sulfate-carbonate solution), FTpulp-KCO, FTpulp-NKCB, FTpulp-NKCA, FTpulp-OrtA, FTpulp.OrtB (all low-temperature alkali sulfate-carbonate solid solutions), FTpulpACL (alkali chloride solid solution), FTpulp-NAKS (alkali sulfide solid solution), and FTpulp-Gsrt ($K_3Na_2(SO_4)_2$- based solid solution). In all calculated cases, FTpulp-Hexa and FTpulp-ACL were the solid stable phases at T_0. The deposits' melting behaviour as a function of temperature is shown in Fig. 1.

The initial melting behaviour of deposits was studied using short-term experiments. The 0-minute experiment had the shortest exposure time, where the probe was removed from the furnace as soon as the furnace reached the temperature set point (see Fig. 2). However, for these short-term experiments, the outer deposit surface was exposed to temperatures higher than the probe set temperature for 30 – 50 min, depending on the chosen temperatures. A typical heating curve for the probe and tube furnace of a 0-minute experiment is shown in Fig. 2.

At point 1 in Fig. 2, the probe reached its set temperature of 450 °C. At this point, cooling of the probe was initiated, maintaining a stable steel temperature. Between points 1 and 2, the furnace temperature increased continuously, while the steel temperature remained at 450 °C. During this time interval, the temperature gradient over the deposit cross-section developed and the outer region of the deposit reached temperatures above its T_0. At point 2, the furnace reached the target temperature of 980 °C. The furnace temperature shown in Fig. 2 represents the temperature right above the outer surface of the synthetic deposit, measured by a thermocouple. This temperature is assumed to correspond to the temperature of the outer deposit surface. The temperature measured by the thermocouple was then used to calculate the amount of melt formed during the experiment. The maximum temperature at the outer deposit surface depended on the chosen steel temperature. The lower the steel temperature, the stronger the cooling effect of the steel and the lower the maximum temperature at the outer deposit surface. A table summarising all experiments and their respective steel temperature, deposit surface temperature, and experimental duration is given in Appendix.

After the experiment, the probe was removed from the furnace and the flow of cooling air was increased to quench the synthetic deposit samples to room temperature. For analysis, the cooled steel rings with the deposits were cast in epoxy resin. The samples were then cut to obtain a cross-section, which was subsequently polished and carbon coated. The samples' morphology and chemical composition were analysed using scanning electron microscopy (SEM) and energy-dispersive X-ray analysis (EDXA).

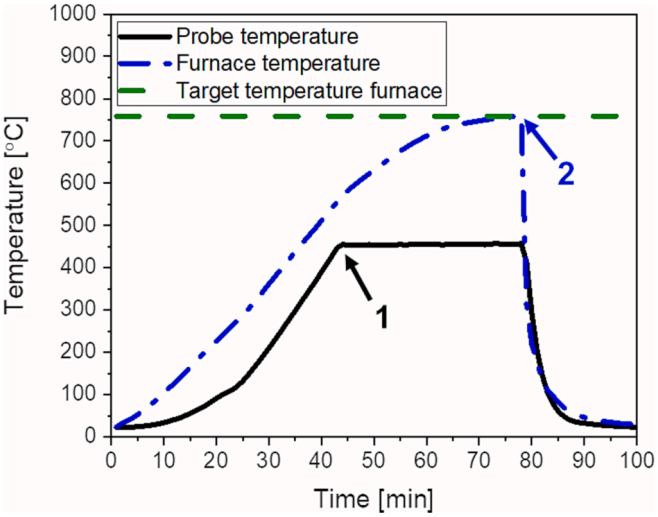

Fig. 2. Profiles of probe and furnace temperature of a 0-minute temperature gradient experiment with the horizontal line indicating the furnace target temperature.

3. Results and discussion

3.1. Differences in deposit morphology

After exposing the synthetic ash deposits to a temperature gradient, differences in their final morphology were observed. Two archetype deposit morphologies developed depending on the initial salt composition and chosen steel and furnace temperatures. Cross-sectional SEM images of the two deposit archetypes are shown in Fig. 3. The figure contains images of synthetic laboratory deposits as well as full-scale superheater deposits, presented in more detail elsewhere [26,27].

In Fig. 3, the steel surface is at the bottom of the images, corresponding to the lowest local temperature within the cross-section. During the exposure, the local deposit temperature increased with the distance from the steel toward the hotter furnace air (flue gas in the case of the superheater deposits). Thus, the local deposit temperature reached its maximum at the top of the image. All SEM images of deposit cross-sections in the present report are oriented the same way as those in Fig. 3. For greyscale SEM images, black represents voids within the deposit. Shades of dark grey correspond to alkali sulfate (and carbonate in the case of actual superheater deposits). Brighter shades of grey correspond to alkali chlorides.

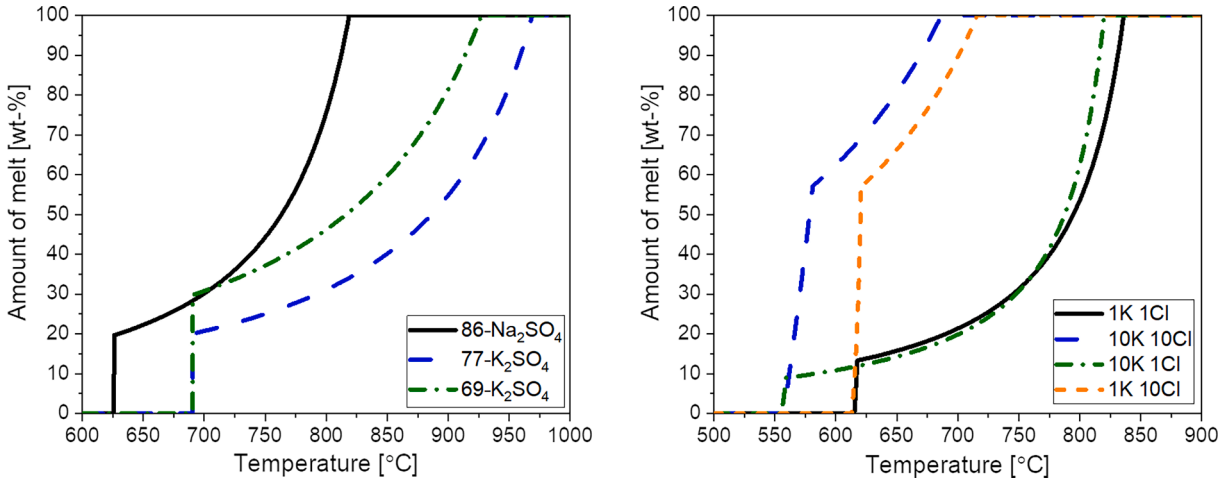

Fig. 1. Melting behaviour of synthetic ash deposits used in present study: binary salt system mixtures (left) and ternary reciprocal salt system mixtures (right).

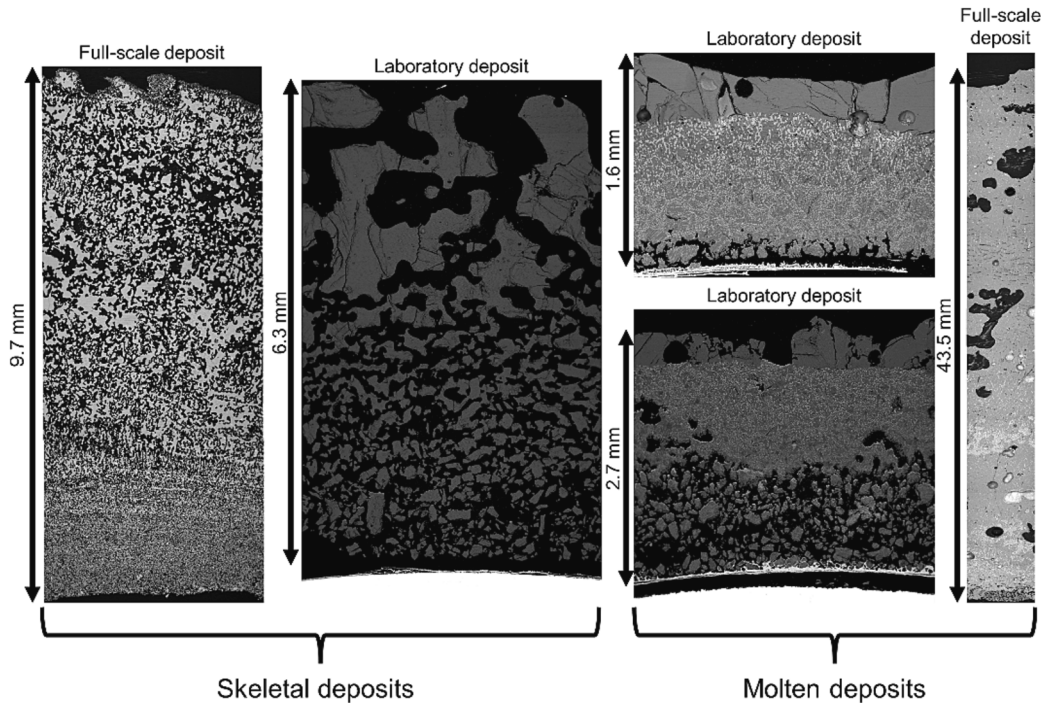

Fig. 3. Examples of laboratory and full-scale deposits for two morphological archetypes: Skeletal full-scale [27] and laboratory deposits on the left and molten full-scale [26] and laboratory deposits on the right.

All deposits in Fig. 3 have a porous region closest to the steel. Only for the low-Cl boiler deposit, sintering is observed throughout the whole cross-section even closest to the steel. The original distinct particles can still be identified in the innermost layer of the low-Cl boiler deposit. The local temperature within the deposit cross-section was the lowest closest to the steel. To avoid direct contact of molten deposit fractions with the steel, material/steam temperatures are typically kept well below the deposit's T_0. Under such conditions, sintering processes are slow, due to the lack of melt. The presence of melt is known to accelerate sintering processes significantly [30]. Thus, no extensive sintering was observed in the low-Cl boiler deposit. However, the smaller particle size of the superheater deposit compared to the laboratory deposits shown in Fig. 3 has been reported to favour sintering [31]. Hence, the low-Cl boiler deposit formed a skeletal morphology throughout the cross-section, despite local temperatures having been below T_0. In addition, single sub-micrometer-sized fume particles tend to agglomerate already in flight, before depositing on the heat transfer surface. Therefore, deposits consisting predominantly of fume particles can form a morphology similar to a sintered deposit. It should be mentioned here that material loss during boiler deposit sampling cannot be ruled out. For porous deposits, especially if unsintered as the local deposit temperature remained below T_0 [32,33], there is an increased risk for particles closest to the steel surface to get lost or destroyed during sampling.

The deposits have apparent morphological differences in the region further away from the steel surface (Fig. 3). The deposits on the left-hand side consist of a network of sintered particles, and the original individual particles can no longer be identified. For all deposits, the measured temperature at the outer surface was above their respective bulk T_0. Thus, the outer deposit regions were partially molten during the exposure. Already small amounts of melt accelerate sintering processes significantly [30]; hence, the deposit morphology changes when local temperatures reach T_0. This morphology will be referred to as "skeletal" and is characterised by a porous network of sintered particles, as seen in the outer region of the deposits on the left of Fig. 3. Depending on the degree of sintering, the original individual particles can no longer be identified, as in the laboratory deposits on the left of Fig. 3.

The local temperature at the outer surface of the deposits on the right in Fig. 3 exceeded T_0 as well. However, the morphology suggests that the temperature was high enough for extensive melt formation. Thus, sufficient melt was present for pore filling, forming the dense morphology seen in Fig. 3. This kind of deposit is referred to as "molten" in further discussion. A molten deposit is characterised by a dense morphology where the original pores of the deposit have been filled by melt. Molten morphologies can still contain inclusions of air, as seen in the molten full-scale deposit in Fig. 3. The amount of melt formed within kraft recovery boiler deposits and the synthetic deposits used in this study depends mainly on their Cl content [17].

In this work, the shortest exposure time was zero minutes, calculated from when the furnace reached the set temperature. Already at such short exposure times, morphological changes in the deposit cross-sections were observed. The temperature logs showed that the outer deposit surface reached temperatures above T_0 already during the heating phase. The formed melt subsequently accelerated morphological changes and a skeletal or molten morphology could already be observed after 0-minute experiments.

A detailed analysis of the elemental composition of molten deposits of ternary reciprocal salts revealed local enrichment in K and Cl toward the steel. Similar observations have also been made in molten, high-Cl boiler deposits [26]. A cross-sectional SEM image of a synthetic deposit enriched in K and Cl toward the steel and the corresponding molar K/(Na + K) and Cl/(Na + K) ratios are given in Fig. 4. The figure also shows an SEM image and elemental molar ratios of a high-Cl deposit obtained directly from a superheater tube of a kraft recovery boiler [26].

The synthetic and boiler deposit has a maximum in the average K/(Na + K) ratio in the molten layer at the interface with the porous region closest to the steel. Each point in the graph gives the average molar ratio value over a horizontal line of pixels. The analysed maximum values were due to the local enrichment in K within the melt. This enrichment enabled the melt to move closer to the steel with time. The main constituent in kraft recovery boiler deposits is Na_2SO_4. In such deposits, the increase in K content decreases the local first melting temperature. The enrichment in K within the melt enables movement of melt toward the steel, to regions where local temperatures are below T_0 of the initially deposited material. A detailed explanation of the mechanism resulting in

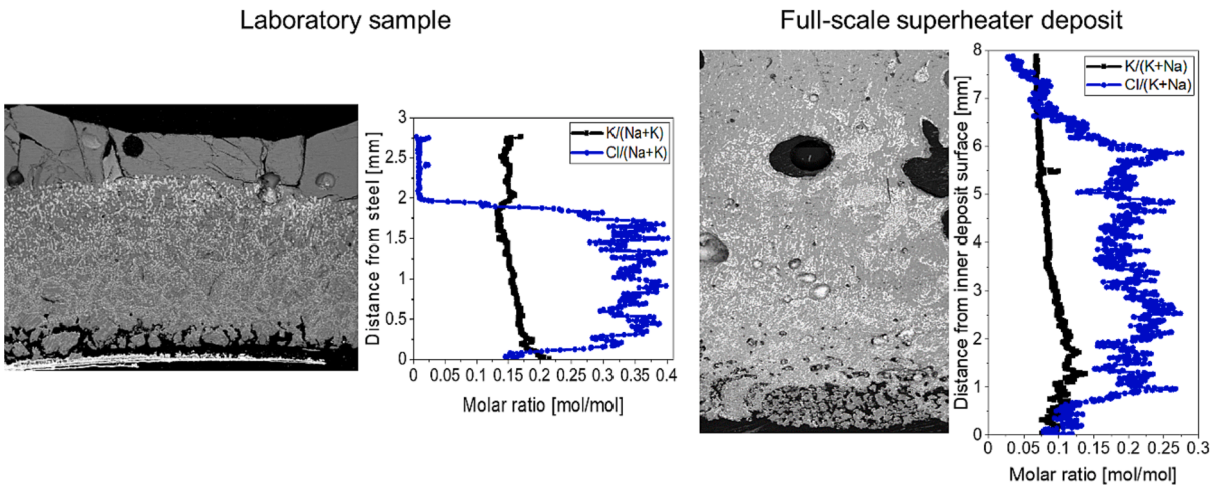

Fig. 4. Greyscale SEM images of molten deposits and corresponding molar K/(Na + K) and Cl/(Na + K) ratios showing local enrichment in K toward the steel; laboratory 10 K 10Cl deposit (left); full-scale superheater deposit (right).

melt movement is given elsewhere [26].

For the laboratory sample shown in Fig. 4, the steel temperature and initial bulk T_0 were 450 °C and 557 °C, respectively. Based on experiments using binary salts, the first estimate of the porous layer thickness for the laboratory sample was approximately 1 mm. However, due to the enrichment in K and the resulting local decrease in T_0, the melt moved closer to the steel before solidifying. Hence the final porous layer thickness of 0.3 mm was significantly thinner than initially estimated. Thus, the experience from earlier experiments utilising binary systems was no longer applicable to more complex ternary reciprocal salt systems. The experiments using ternary reciprocal salts confirmed the observations made earlier in the actual boiler deposits.

For binary salts, a local change in deposit composition due to element enrichment does not affect T_0 due to their eutectic nature. Nevertheless, local element enrichment within the molten phase has also been reported for binary systems [15,24,25]. The composition of the molten phase approaches the eutectic composition toward the interface between the molten and porous layer [15,24,25]. However, this does not change the local first melting temperature and no significant decrease in the thickness of the porous layer has been reported when using binary salts.

A molten phase moving closer toward the steel can significantly increase the risk for corrosion [34], as melt getting in direct contact with the steel surface causes severe melt-induced corrosion. Furthermore, due to the deposit melting, the location of T_0 within the deposit cross-section moves closer toward the steel and the steepness of the temperature gradient over the porous region underneath increases. The steeper temperature gradient over the porous deposit region subsequently accelerates deposit ageing via diffusional transport of alkali chloride vapours toward the steel [35].

No local element enrichment in K or Cl toward the steel took place in the skeletal deposit regions. The amount of melt present was insufficient

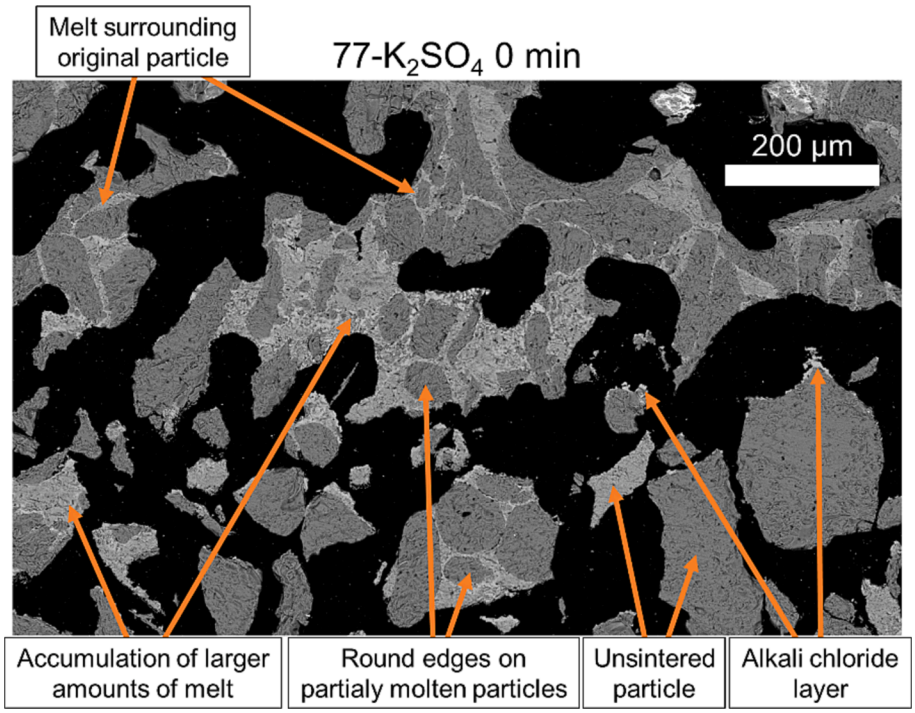

Fig. 5. Detailed view on skeletal region of a 0-minute experiment highlighting its main features.

for pore filling and movement of melt toward the steel. However, the outer part of skeletal deposits experienced temperatures above T_0, and the formed melt accelerated sintering, hence the formation of the skeletal region. The impact of melt on the formation of the skeletal deposit morphology is highlighted in Fig. 5.

The sintering of salt systems proceeds predominantly via two main mechanisms. In the first, volatile compounds in the deposit evaporate and condense at contact points or close contact areas between distinct particles within the deposit [36]. The second mechanism involves solid-state diffusion within the deposit particles [36]. Both mechanisms result in the formation of necks between the single deposit particles. These necks then grow further, up to a point at which the original particles can no longer be identified. The presence of melt greatly accelerates the sintering process [30], as it accumulates at contact points and supports neck formation. In this case, the mechanism is referred to as liquid phase sintering. For the skeletal region, seen in the short-term deposits in this work, the sintering process and formation of the skeletal morphology were accelerated by the presence of melt. Thus, as explained above, a skeletal layer formed already during the 0-minute experiment.

In the deposit shown in Fig. 5, locally high concentrations of alkali chloride were observed in the skeletal region. These Cl-rich regions are an indicator for partial melting of the deposit to have taken place. For all synthetic deposit compositions used in this work, and recovery boiler deposits in general, all Cl present in the deposit is incorporated in the molten phase as soon as T_0 is reached. For the skeletal deposit in Fig. 5, the amount of melt formed was insufficient to fill the pores. Thus no molten morphology formed. Instead, the formed melt accumulated at contact points of distinct particles, where it accelerated the sintering process. In some cases, Cl-rich melt seemed to surround deposit particles. The round edges of these melt-surrounded particles were an additional indicator of partial melting of the deposit.

With increasing exposure time, alkali chlorides within the melt are prone to evaporate. Alkali chloride vapours diffuse either into the furnace/flue gases or toward the colder region in the deposit, closer to the steel. Diffusion toward the steel is driven by the gas-phase concentration gradient [24,25]. At lower local temperatures, the alkali chlorides form typical layers on the furnace-facing sides of particles via condensation [24,25]. Thin layers of alkali chloride were identified after the 0-minute experiments, as shown in Fig. 5. With increasing exposure time, the alkali chloride layers grew in thickness and the skeletal deposit

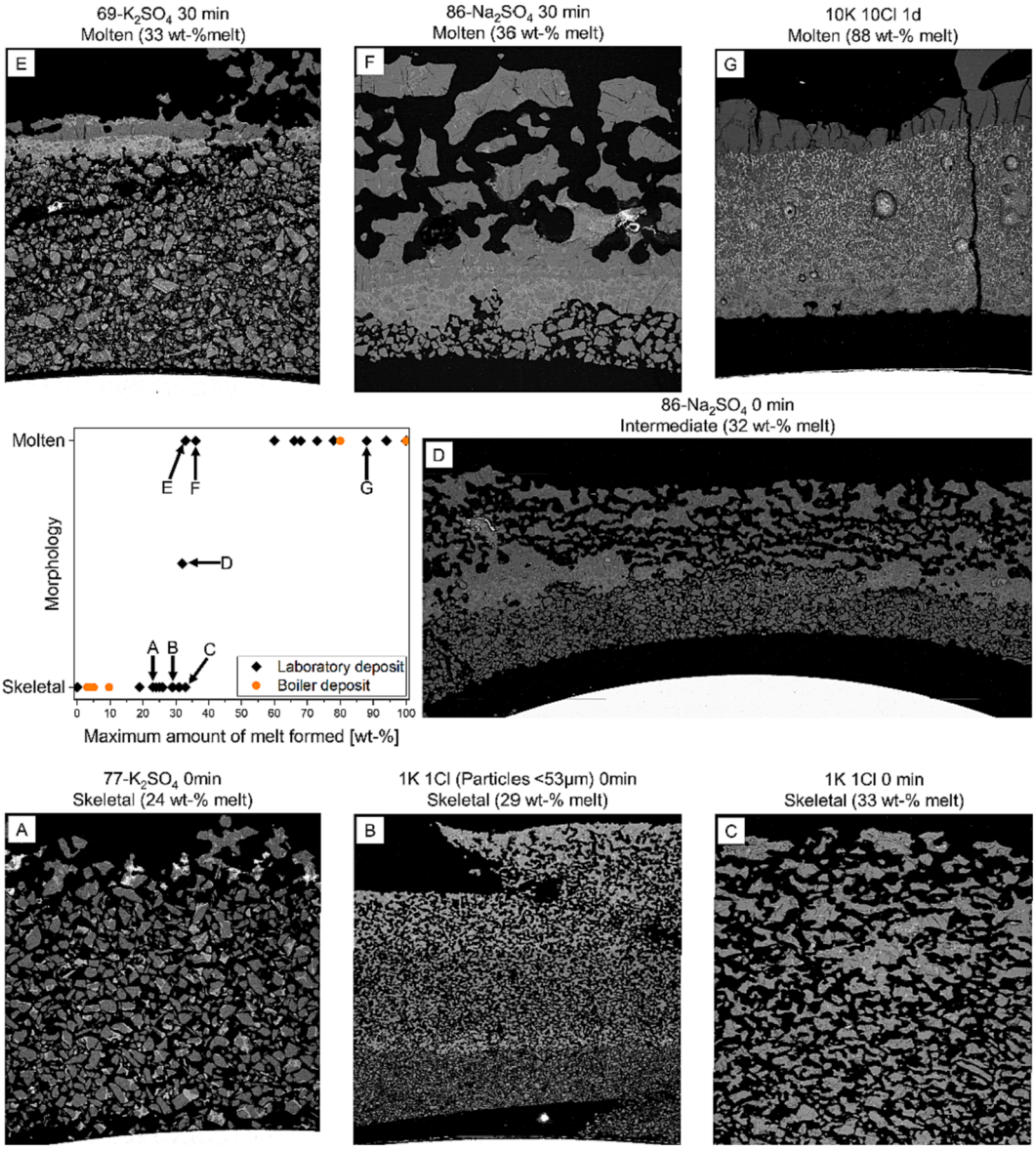

Fig. 6. Summary of available data on final deposit morphology as a function of the amount of melt. Selected SEM images depicting skeletal (A, B, and C); intermediate (D); molten deposits (E, F, and G). The orange dots are for kraft recovery boiler deposits.

was depleted in Cl.

The differences in morphology and ageing behaviour of the two deposit archetypes have a significant impact on the corrosivity and removability of the deposits. Therefore, being able to predict the final deposit morphology can help significantly in predicting and preventing operational issues caused by deposits. In the following, the decisive parameter causing a change in deposit morphology, as well as a threshold for when the change in deposit morphology takes place will be identified.

3.2. Transition from skeletal to molten morphology

The results presented above imply that the final deposit morphology depends on the amount of melt formed within the deposit. SEM images of 33 deposit cross-sections were analysed to identify the threshold for the melt fractions, at which a molten deposit morphology forms. The samples comprise short- and long-term temperature gradient laboratory experiments, using binary and ternary reciprocal salt systems. In addition, actual superheater deposits from two kraft recovery boilers were analysed. Based on the deposit morphology, the results were classified into three categories: skeletal, molten, and intermediate. The graph showing the morphology as a function of the maximum amount of melt in Fig. 6 summarises the deposit classification. The figure also shows SEM images of selected deposit cross-sections illustrating the changes in deposit morphology with changing melt fractions. SEM images of all studied laboratory deposit cross-sections are given in the supplementary material.

The maximum amount of melt in the deposits was calculated based on the highest temperature measured by the thermocouple at the outer deposit surface. For deposits with an initial low Cl content (1 wt-%), SEM analysis revealed evaporation of a significant share of Cl into the furnace during the heating phase which affects the deposit's melting behaviour. Hence, for deposits of a low initial Cl content, the maximum amount of melt was determined based on SEM analysis data instead of its initial composition. For deposits of a higher initial Cl content, evaporation of Cl did not have a similar impact on the melting behaviour.

The parameters varied in the laboratory deposits summarised in the graph in Fig. 6 were exposure time, set temperatures of probe and furnace, and deposit composition. Furthermore, the impact of different initial particle sizes on the final deposit morphology was studied. Fig. 6 also contains data from boiler deposits. The superheater deposits are marked with orange circles in the graph. All skeletal superheater deposits were obtained from a Finnish kraft recovery boiler [27], while all superheater deposits of a molten morphology were obtained from a Brazilian kraft recovery boiler [26]. The Brazilian deposits formed a molten morphology due to a significantly higher Cl content compared to the Finnish deposits.

The amount of melt formed in the skeletal deposits increased from A to C (Fig. 6). No molten layer formed in these deposits. The deposit in Image A had the lowest melt fraction of the selected deposits. Only a thin skeletal layer formed at its outer surface and most of the deposit remained porous. The results imply that the thickness of the skeletal layer did not depend on the amount of melt but on the differences in T_{steel}, deposit T_0, and $T_{outer\ surface}$. Only the region of the deposit where the local temperature exceeded T_0 formed a skeletal morphology. For the deposit in image A, the maximum temperature during the experiment was only 50 °C above T_0; thus, only a thin layer on the outer deposit surface experienced temperatures above T_0.

Image B in Fig. 6 shows a deposit consisting of a smaller particle size fraction. Niemi et al. [35] reported a decrease in particle size to have resulted in the formation of a molten deposit morphology, with all other parameters unchanged. Reducing the particle size decreases the pore size of void areas but does not affect the deposit's overall porosity. Further, liquid phase sintering eliminates smaller pores more efficiently due to higher capillary forces [30,37]. As a reduction of the particle size affects the sintering process, the formation of a molten morphology does not exclusively depend on the amount of melt in the deposit. The threshold amount of melt required to form a molten morphology can vary. Deposit melting is a highly complex process and is affected by several parameters simultaneously. Furthermore, deposit densification can take place via pathways other than pore filling by melt [38], which can eventually result in a morphology similar to molten deposits. However, these mechanisms are typically much slower and of no relevance for the short-term experiments presented here.

In this work, only reducing the particle size did not change the deposit morphology. The increase in capillary forces due to smaller particles has a lesser impact on the final deposit morphology than the amount of melt [37]. Therefore, no change in the final deposit morphology was observed for deposit B.

Image C in Fig. 6 shows sporadically distributed, larger agglomerates of particles throughout the outer region of the cross-section. The analysis suggests that these agglomerates consist of several particles sintered together by a small amount of melt, rather than formed by a larger amount of melt in the outer deposit.

Significant differences were identified between deposits C and D in Fig. 6. Larger accumulations of melt were observed in the middle of deposit D. Within these melt accumulations, phase separation and enrichment in Cl toward the steel was identified, a mechanism that was earlier associated with the formation of larger amounts of melt. A similar phase separation was not seen for the agglomerates in deposit C. Therefore, the areas of molten morphology in deposit D were assumed to have formed due to the accumulation of melt. However, the amount of melt was not sufficient to form a molten morphology, covering the whole cross-section of the deposit. The outer region still resembled a skeletal structure. As the deposit showed properties of both morphological archetypes it was classified as an intermediate morphology between skeletal and molten.

Images E, F, and G in Fig. 6 are examples of molten deposit morphologies. Image E shows the deposit with the lowest calculated melt fraction of all molten deposits. Only a thin molten layer formed on the outer deposit surface, and most of the deposit underneath the molten layer remained porous. The relatively thin molten layer indicates that the amount of melt formed during the experiment was just above the threshold to form a molten deposit morphology. Phase separation and Cl-enrichment in the melt toward the steel surface were identified. As deposit E was a binary salt, no decrease in T_0 due to local element enrichment and subsequent movement of melt toward the steel took place. Hence only a thin molten layer formed on the outer deposit surface.

The molten layer of deposit F is significantly thicker compared to deposit E. Furthermore, a skeletal region above the molten layer suggests that melt, initially formed at the outer part of the deposit, moved toward the steel where it accumulated and formed a molten morphology. Two conditions must be met for the melt to move toward the steel. First, the amount of melt formed must be sufficient to move toward the steel due to capillary and gravitational forces. Second, the temperature closer to the steel must be above the melt's solidification temperature. A temperature profile develops over the cross-section with prolonged exposure. Accordingly, T_0 in the deposit moves closer toward the steel. Furthermore, the sintering and melting of the deposit increase the thermal conductivity [39] in the outer deposit region, additionally moving T_0 closer to the steel.

The experimental conditions for deposits D and F were identical, except for the longer exposure time for deposit F. The experimental setup did not allow a precise temperature adjustment at the outer deposit surface. Therefore a slightly higher temperature was recorded for deposit F than D. The melt fraction in the molten deposit F was 4 wt-% higher than in deposit D. The slight increase in melt fraction resulted in a significant change in the deposit morphology. The morphology of deposit F supports the classification of deposit D as intermediate since the small increase in the melt fraction from D to F caused a molten morphology to form. Deposits D and F gave additional proof of the

amount of melt to be the decisive parameter affecting the final deposit morphology. Already a small increase in the melt fraction, under the same experimental conditions, resulted in a significant change in the deposit morphology.

In deposit G in Fig. 6, a significantly larger amount of melt (88 wt-%) formed during the experiment. The synthetic salt used in this experiment was of a ternary reciprocal system. Temperature gradient-induced local enrichment in K enabled the melt to move closer toward the steel before solidifying. Therefore, melt was present in regions where local temperatures were well below the initial bulk T_0. The pores in the deposit closer to the steel were filled by melt and eliminated. The gap between the steel and the molten region seen in deposit G is due to the sample preparation after the exposure. The epoxy resin used to fix the deposit detached and separated it from the steel surface. This issue was observed for several of the laboratory experiments. However, a loss of the porous layer during sample preparation, especially cutting the deposit to obtain a cross-section, cannot be ruled out to have resulted in the formation of the gap between the molten deposit and the steel.

The data summarized in the graph in Fig. 6 indicates that the morphology changed from skeletal to molten when approximately 30 wt-% melt had formed within the deposit. A melt fraction of 30 wt-% was sufficient for the liquid to fill the void areas within the deposit, resulting in a molten morphology. This melt fraction agrees with the general understanding of liquid phase sintering: approximately 30 vol-% liquid is typically required to fill all voids of a porous structure [30]. Furthermore, when considering various packing models of spheres, the identified melt fraction of about 30 wt-% lies within the void area range of ordered close packings (26 vol-%) and random close packings (36 vol-%) [40]. The packing models are based on spheres of equal size, whereas the deposit particle size ranged between 53 and 250 μm, and the particles were of non-uniform shape. However, the suggested amount of approximately 30 wt-% melt for a molten deposit to form is still in good agreement with the packing models of spheres and the liquid phase sintering theory.

As mentioned in the discussion above, several other parameters such as deposit particle size, deposit porosity, the viscosity of the molten phase, or morphological changes affecting the deposit temperature profile influence the melting behaviour of deposits. However, based on the observations made in the present study, all these other parameters were identified as having only a minor impact on the final deposit morphology. Thus, the maximum amount of melt formed in a deposit is identified as the decisive parameter determining its final morphology.

As a continuation of this work, the influence of other parameters on the melting behaviour and thus the final deposit morphology can be studied in more detail. A possible next step can be the extension of the experimental matrix into utilising deposits of compositions other than those relevant to kraft recovery boilers. Furthermore, the impact of the presence of SO_2 or H_2O in the gas phase can be studied to identify to which extent interactions of the deposit and compounds present in the gas phase affect the final deposit morphology.

The results presented above can help in predicting the ageing behaviour of deposits more accurately. The identified threshold amount of melt can be utilised as an additional input for deposition models, that also take subsequent deposit ageing into account. By distinguishing between a skeletal and molten deposit morphology, the ageing behaviour and changes in the local chemical composition of deposits and therewith associated operational problems can be modelled more accurately. This is valuable data for both boiler operators and manufacturers and can help in preventing severe melt-induced corrosion. Furthermore, information on the evolution of the deposit morphology can be utilised when scheduling sootblowing. The better the knowledge of deposits and how they change in their local chemistry and morphology during boiler operation, the more efficiently sootblowing cycles can be scheduled.

4. Conclusions

In short-term laboratory experiments, synthetic ash deposits of compositions characteristic for kraft recovery boilers were exposed to a temperature gradient to study the initial melting behaviour of deposits. Two archetype deposit morphologies with differences in their ageing behaviour emerged. The main findings can be summarised as follows.

- The governing parameter determining the final deposit morphology was identified to be the maximum amount of melt formed within the deposit, with other parameters investigated having only a minor impact on the final deposit morphology. The threshold for a change in the final deposit morphology is at about 30 wt-% melt formed in the deposit.
- A skeletal morphology forms if the amount of melt remains below 30 wt-%. Skeletal deposits are characterized by a sintered, but still porous morphology. If small amounts of melt are formed in the deposit, a skeletal morphology can already form after very short exposure times as the sintering process is accelerated significantly by the presence of melt.
- A molten morphology forms when the maximum amount of melt exceeds 30 wt-%. Molten deposits are characterized by a dense, non-porous layer that forms due to melt filling the voids of the initially porous deposit.
- Differences in the ageing behaviour of the two morphological archetypes were identified. The governing ageing mechanism for skeletal deposits is the diffusional transport of vapours toward the steel, induced by a temperature gradient. In molten deposits, movement of melt toward the steel coupled with element enrichment was seen, causing a decrease in the local first melting temperature.
- The presented results provide new information on deposit ageing mechanisms and their impact on superheater corrosion and deposit removability. The new insights aim to help in identifying the governing deposit ageing mechanisms based on deposit morphology, which facilitates the identification of regions in a boiler at an increased risk for deposit-induced problems to occur. This in turn helps to better predict and avoid deposit-induced issues in boilers.

CRediT authorship contribution statement

Roland Balint: Writing – original draft, Investigation, Data curation, Conceptualization. **Markus Engblom:** Writing – review & editing, Validation, Supervision, Project administration, Investigation, Funding acquisition, Conceptualization. **Jonne Niemi:** Writing – review & editing, Validation, Supervision, Conceptualization. **Mikko Hupa:** Writing – review & editing, Validation, Funding acquisition. **Leena Hupa:** Writing – review & editing, Funding acquisition.

Declaration of Competing Interest

The authors declare that they have no known competing financial interests or personal relationships that could have appeared to influence the work reported in this paper.

Data availability

SEM images of the analysed deposits are provided as supplementary material and were uploaded at the attach file step

Acknowledgements

This work was financed by a research grant awarded by the Fortum Foundation, Finland [Application number 20190123] and the Åbo Akademi University Graduate School in Chemical Engineering. This work has been partly carried out within the Åbo Akademi CLUE2 Research Consortium (2017-2022). Support from ANDRITZ Oy, Valmet

Technologies Oy, UPM-Kymmene Oyj, Metsä Fibre Oy, and International Paper Inc. is gratefully acknowledged. Additional support from the Research Council of Finland project "New insights on the effects of temperature gradients on high temperature corrosion" [Decision number 338322] is highly appreciated. We want to thank Linus Silvander for carrying out SEM/EDXA analyses.

Appendix

A) Summary of laboratory temperature gradient experiments containing deposit name, steel temperature, maximum temperature at outer deposit surface, and exposure time

Salt name	Steel temperature [°C]	Maximum deposit temperature [°C]	Exposure time [h]
1 K 1Cl	450	753	72
1 K 1Cl	450	685	120
77-K_2SO_4	450	726	0.5
77-K_2SO_4	450	737	0
1 K 1Cl	500	767	0
1 K 10Cl	400	618	24
10 K 1Cl	450	731	120
10 K 1Cl	450	732	168
1 K 1Cl (<53 μm)	500	767	0
77-K_2SO_4	500	796	24
86-Na_2SO_4	450	712	0
69-K_2SO_4	450	731	0.5
1 K 1Cl	550	780	0
69-K_2SO_4	450	749	0
86-Na_2SO_4	450	725	0.5
10 K 10Cl	400	593	336
10 K 10Cl	400	611	120
10 K 10Cl	400	617	168
1 K 10Cl	400	666	240
10 K 10Cl	400	631	4
10 K 10Cl	400	643	120
10 K 10Cl	400	666	24
10 K 10Cl	400	677	4
1 K 10Cl	450	735	72
1 K 10Cl	450	737	168
10 K 10Cl	450	747	0
10 K 10Cl	450	757	72

Appendix A. Supplementary data

Supplementary data to this article can be found online at https://doi.org/10.1016/j.fuel.2023.130386.

references

[1] Vakkilainen EK. Kraft recovery boilers - Principles and practice. Suomen Soodakattilayhdistys ry 2005.
[2] Mikkanen P, Kauppinen EI, Pyykönen J, Jokiniemi JK, Aurela M, Vakkilainen EK, et al. Alkali salt ash formation in four Finnish industrial recovery boilers. Energy Fuel 1999;13:778–95. https://doi.org/10.1021/ef980189o.
[3] Capablo J. Formation of alkali salt deposits in biomass combustion. Fuel Process Technol 2016;153:58–73. https://doi.org/10.1016/j.fuproc.2016.07.025.
[4] Tran HN, Reeve DW, Barham D. Formation of kraft recovery boiler superheater fireside deposits. Pulp and Paper Canada 1983;84:36–41.
[5] Kleinhans U, Wieland C, Frandsen FJ, Spliethoff H. Ash formation and deposition in coal and biomass fired combustion systems: Progress and challenges in the field of ash particle sticking and rebound behavior. Prog Energy Combust Sci 2018;68:65–168. https://doi.org/10.1016/j.pecs.2018.02.001.
[6] Niu Y, Tan H, Hui S. Ash-related issues during biomass combustion: Alkali-induced slagging, silicate melt-induced slagging (ash fusion), agglomeration, corrosion, ash utilization, and related countermeasures. Prog Energy Combust Sci 2016;52:1–61. https://doi.org/10.1016/j.pecs.2015.09.003.
[7] Baxter LL. Ash Deposit Formation and Deposit Properties 2000. https://doi.org/10.2172/760515.
[8] Wessel RA, Baxter L, Shaddix C, Verrill C, Frederick WJJ, Lien S, et al. Particle formation and deposition in recovery boilers. TAPPI Fall Technical Conference and Trade Fair 2002:315–28.
[9] P. Mikkanen Fly ash particle formation in kraft recovery boilers. 2000.
[10] Grabke HJ, Reese E, Spiegel M. The effects of chlorides, hydrogen chloride, and sulfur dioxide in the oxidation of steels below deposits. Corros Sci 1995;37:1023–43. https://doi.org/10.1016/0010-938X(95)00011-8.
[11] Uusitalo MA, Vuoristo PMJ, Mäntylä TA. High temperature corrosion of coatings and boiler steels below chlorine-containing salt deposits. Corros Sci 2004;46:1311–31. https://doi.org/10.1016/j.corsci.2003.09.026.
[12] Karlsson A, Moller PJ, Johansen V. IRON and steel corrosion in a system of O2, SO2, and alkali chloride. The formation of low melting point salt mixtures. Corros Sci 1990;30:153–8. https://doi.org/10.1016/0010-938X(90)90069-H.
[13] Lindberg D, Backman R, Chartrand P. Thermodynamic evaluation and optimization of the (NaCl + Na2SO4+ Na2CO3+ KCl + K2SO4+ K2CO3) system. J Chem Thermodyn 2007;39:1001–21. https://doi.org/10.1016/j.jct.2006.12.018.
[14] Karlemo C. Non-process elements in the recovery cycle of six Finnish Kraft pulp mills. Åbo Akademi University; 2019. Master's Thesis.
[15] Niemi J, Balint R, Engblom M, Lehmusto J, Lindberg D. Temperature-gradient-driven aging mechanisms in alkali-bromide- And sulfate-containing ash deposits. Energy Fuel 2019;33:5883–92. https://doi.org/10.1021/acs.energyfuels.8b04199.
[16] Tran H, Gonsko M, Mao X. Effect of composition on the first melting temperature of fireside deposits in recovery boilers. Tappi J 1999;82:93–100.
[17] Reeve DW, Tran HN, Barham D. The effluent-free bleached kraft pulp mill - Part XI Morphology, chemical and thermal properties of recovery boiler superheater fireside deposits. Pulp & Paper Canada 1981;82:T315–20.
[18] A. Costa D. Silva F. Abelha Cenibra CNSA. EXPERIENCE OF RECOVERY BOILER SUPERHEATER CORROSION AT CENIBRA. International Chemical Recovery Conference - ICRC, Halifax, Canada: 2017.
[19] Jensen PA, Frandsen FJ, Hansen J, Dam-Johansen K, Henrisken N, Hörlyck S. SEM investigation of superheater deposits from biomass-fired boilers. Energy Fuel 2004;18:378–84. https://doi.org/10.1021/ef030097l.
[20] Tang X, Liu Q, Wang T. Ash deposition characteristics during oxy-fuel combustion of biomass in a drop tube furnace. Biomass Convers Biorefin 2023. https://doi.org/10.1007/s13399-023-04020-3.
[21] Hansen LA, Nielsen HP, Frandsen FJ, Dam-Johansen K, Hörlyck S, Karlsson A. Influence of deposit formation on corrosion at a straw-fired boiler. Fuel Process Technol 2000;64:189–209. https://doi.org/10.1016/S0378-3820(00)00063-1.

[22] Lapuerta M, Acosta A, Pazo A. Fouling deposits from residual biomass with high sodium content in power plants. Energy Fuel 2015;29:5007–17. https://doi.org/10.1021/acs.energyfuels.5b00356.
[23] Zhou H, Jensen PA, Frandsen FJ. Dynamic mechanistic model of superheater deposit growth and shedding in a biomass fired grate boiler. Fuel 2007;86:1519–33. https://doi.org/10.1016/j.fuel.2006.10.026.
[24] Lindberg D, Niemi J, Engblom M, Yrjas P, Laurén T, Hupa M. Effect of temperature gradient on composition and morphology of synthetic chlorine-containing biomass boiler deposits. Fuel Process Technol 2016;141:285–98. https://doi.org/10.1016/j.fuproc.2015.10.011.
[25] Niemi J, Lindberg D, Engblom M, Hupa M. Simultaneous melt and vapor induced ash deposit aging mechanisms – Mathematical model and experimental observations. Chem Eng Sci 2017;173:196–207. https://doi.org/10.1016/j.ces.2017.07.041.
[26] Balint R, Engblom M, Niemi J, da Costa DS, Lindberg D, Yrjas P, et al. Temperature gradient induced changes within superheater ash deposits high in chlorine. Energy 2021;226:120439. https://doi.org/10.1016/j.energy.2021.120439.
[27] Balint R, Engblom M, Niemi J, Lindberg D, Saarinen T, Rautala J, et al. Morphological and chemical differences within superheater deposits from different locations of a black liquor recovery boiler. Energy 2023;267:126576. https://doi.org/10.1016/j.energy.2022.126576.
[28] Balint R, Engblom M, Vainio E, Laurén T, Niemi J, Rautala J, et al. Changes in chlorine content over time – Probe deposit sampling in a Finnish kraft recovery boiler. Fuel 2023;340:127599. https://doi.org/10.1016/j.fuel.2023.127599.
[29] CW. Bale E. Bélisle P. Chartrand SA. Decterov G. Eriksson AE. Gheribi et al. FactSage thermochemical software and databases, 2010-2016. Calphad: Computer Coupling of Phase Diagrams and Thermochemistry 54 2016 35 53 10.1016/j.calphad.2016.05.002.
[30] German RM, Suri P, Park SJ. Review: Liquid phase sintering. J Mater Sci 2009;44:1–39. https://doi.org/10.1007/s10853-008-3008-0.
[31] Skrifvars B-J, Hupa M, Hyöty P. Composition of recovery-boiler dust and its effect on sintering. Tappi J 1991;74:185–9.
[32] Laxminarayan Y, Nair AB, Jensen PA, Wu H, Frandsen FJ, Sander B, et al. Tensile adhesion strength of biomass ash deposits: Effect of the temperature gradient and ash chemistry. Energy Fuel 2018;32:4432–41. https://doi.org/10.1021/acs.energyfuels.7b03114.
[33] Mao X, Tran H, Cormack DE. Effects of chemical composition on the removability of recovery boiler fireside depositS. TAPPI JOURNAL 2001;84.
[34] Hupa M, Karlström O, Vainio E. Biomass combustion technology development – It is all about chemical details. Proc Combust Inst 2017;36:113–34. https://doi.org/10.1016/j.proci.2016.06.152.
[35] Niemi J, Engblom M, Laurén T, Yrjas P, Lehmusto J, Hupa M, et al. Superheater deposits and corrosion in temperature gradient – Laboratory studies into effects of flue gas composition, initial deposit structure, and exposure time. Energy 2021;228. https://doi.org/10.1016/j.energy.2021.120494.
[36] Frederick WJ, Ling A, Tran HN, Lien SJ. Mechanisms of sintering of alkali metal salt aerosol deposits in recovery boilers. Fuel 2004;83:1659–64. https://doi.org/10.1016/j.fuel.2004.02.005.
[37] Lee SM, Kang SJL. Theoretical analysis of liquid-phase sintering: Pore filling theory. Acta Mater 1998;46:3191–202. https://doi.org/10.1016/S1359-6454(97)00489-8.
[38] Techakijkajorn U, Frederick WJ, Tran HN. Sintering and densification of recovery boiler deposits: Laboratory data and a rate model. J Pulp Pap Sci 1999;25:73–80.
[39] Zbogar A, Frandsen FJ, Jensen PA, Glarborg P. Heat transfer in ash deposits: A modelling tool-box. Prog Energy Combust Sci 2005;31:371–421. https://doi.org/10.1016/j.pecs.2005.08.002.
[40] Berryman JG. Random close packing of hard spheres and disks. Phys Rev A 1983;27:1053–61. https://doi.org/10.1103/PhysRevA.27.1053.